Earth Evolution Sciences, Vol. 16, pp. 2–13, March 1, 2022

Phase equilibrium modeling and pressure–temperature evolution of the Sanbagawa pelitic schists in Kanto Mountains, Central Japan

Yusuke Kuribara [a], Toshiaki Tsunogae [b,c,*]

[a] *Graduate School of Life and Environmental Sciences, University of Tsukuba, Ibaraki 305-8572, Japan*
[b] *Faculty of Life and Environmental Sciences, University of Tsukuba, Ibaraki 305-8572, Japan*
[c] *Department of Geology, University of Johannesburg, Auckland Park 2006, Republic of South Africa*

[*] *Corresponding author (tsunogae@geol.tsukuba.ac.jp)*

Abstract

We report new pressure and temperature (*P–T*) data of a pelitic schist from Yoshii area, Gunma Prefecture, for evaluating the peak metamorphic condition of the Sanbagawa metamorphic belt in Kanto Mountains. The studied sample contains the mineral assemblage of quartz + phengite + albite + biotite + epidote + garnet + ilmenite, which is a common mineral assemblage of pelitic schists in the highest-grade zone (biotite zone) of this region. The peak *P–T* condition for the assemblage has been inferred based on phase equilibrium modeling in MnNCKFMASHT system as 470–550°C/6.0–9.5 kbar, which is nearly consistent with the results of garnet-phengite geothermometry (460–580°C) applied to the same sample. The results are also comparable with previous *P–T* estimates from the biotite zone in Kanto Mountains as well as those of the albite-biotite zone in central Shikoku. The results of our modeling also suggest that the peak metamorphism was followed by decompressional cooling toward the stability field of a retrograde assemblage (chlorite + biotite + muscovite + epidote + ilmenite + quartz + albite + titanite) at <470°C/<7 kbar, possibly along a clockwise *P–T* path. The results of this study therefore confirmed eastward decrease of metamorphic grade within the Sanbagawa metamorphic belt.

Keywords: Petrology; *P–T* condition; Pseudosection; MnNCKFMASHT system; Garnet-phengite geothermometry

Introduction

The Sanbagawa metamorphic belt, which extends about 800 km from east (Kanto Mountains) to west (Kyushu) (Fig. 1a) along the northern margin of the Outer Zone in southwest Japan, is regarded as an example of high-pressure and low-temperature (high *P*/*T*) type metamorphic belts formed by complex subduction-accretion processes in western Pacific region during Cretaceous (e.g., Miyashiro, 1961; Isozaki and Itaya, 1990; Enami, 1994). Numerous petrological, geochronological, and structural studies have been performed on various schistose rocks in the Sanbagawa belt, particularly focusing on *P–T* evolution of the rocks and tectonics of the region. However, such previous investigations are mainly performed on the western part of the belt in central Shikoku where the grade of metamorphism is higher than the other regions (e.g., Banno, 1964; Kurata and Banno, 1974; Higashino, 1975, 1990; Enami, 1983, 1994). In contrast, limited studies have been carried out on the Sanbagawa schists in Kanto Mountains (Fig. 1a) which corresponds to the eastern end of the belt (e.g., Toriumi, 1977; Hirajima, 1989; Kouketsu and Shimizu, 2014).

Pelitic and mafic schists with minor psammitic, ultramafic, and siliceous schists are dominant lithologies in Kanto Mountains (e.g., Yano and Tagiri, 1998; Abe et al., 2001). The region is subdivided into three zones; chlorite zone, garnet zone, and biotite zone from low grade to high grade and from south to north based on the occurrence of various index minerals (e.g., Miyashita, 1998; Abe et al., 2001; Fig. 1b). Toriumi (1977) estimated *P–T* condition of 350–400°C/6–7 kbar based on pyrite-sphalerite-pyrrhotite equilibria in pelitic schists collected from the chlorite zone. The peak metamorphic condition of this region has been estimated as 460–540°C/7–12 kbar using carbon isotopic fractionation between calcite and graphite in Fe-Mn-rich nodule from the biotite zone (Hirajima, 1989). Kouketsu and Shimizu (2014) estimated peak metamorphic temperatures of the chlorite zone (360–400°C), the garnet zone (420–450°C), and the biotite zone (460–510°C) based on Raman carbonaceous material thermometer. Inui et al. (2017) also obtained consistent peak metamorphic temperatures of ~400–450°C using the Raman spectra analysis of carbonaceous materials from Nagatoro region. Inui and Tanifuji (2018) examined low-grade garnet-bearing pelitic schists from Nagatoro region, and discusses that the occurrence of garnet is strongly controlled by bulk-rock chemistry. In this study, we report new petrological and *P–T* data of the Sanbagawa pelitic schists from Yoshii area in Gunma

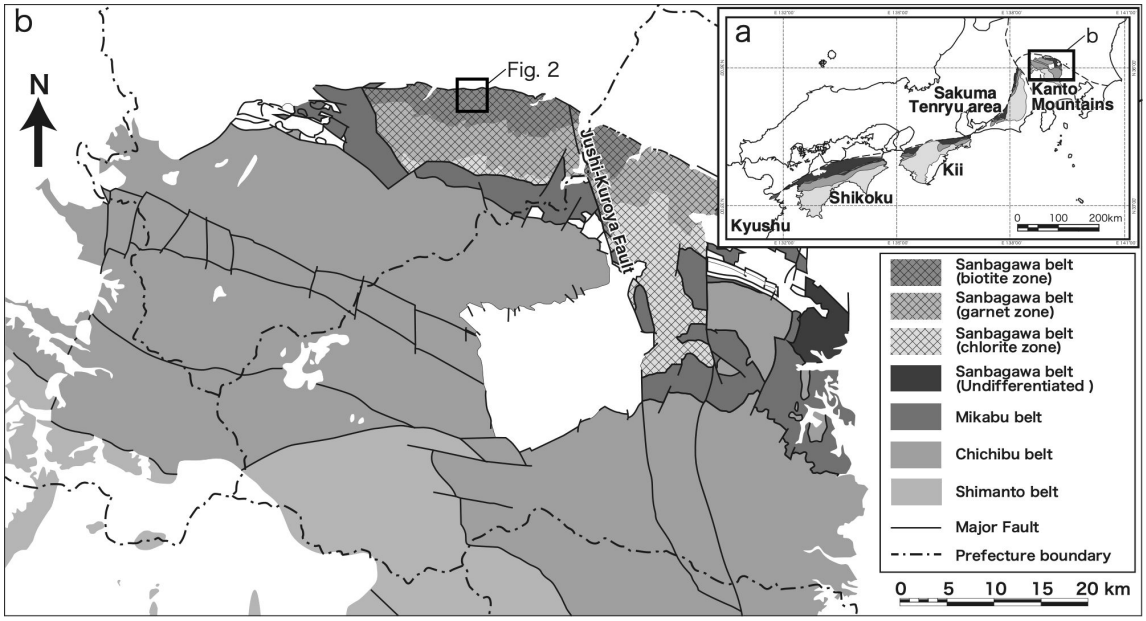

Fig. 1. (a) Tectonic division of the Outer Zone of Southwest Japan. (b) Geological map of the Sanbagawa Belt in Kanto Mountains (modified after Sakamoto et al., 1987; Sudo et al., 1991; Makimoto and Takeuchi, 1992; Yano and Tagiri, 1998; Nakano et al., 1998; Abe et al., 2001; Ozaki et al., 2002).

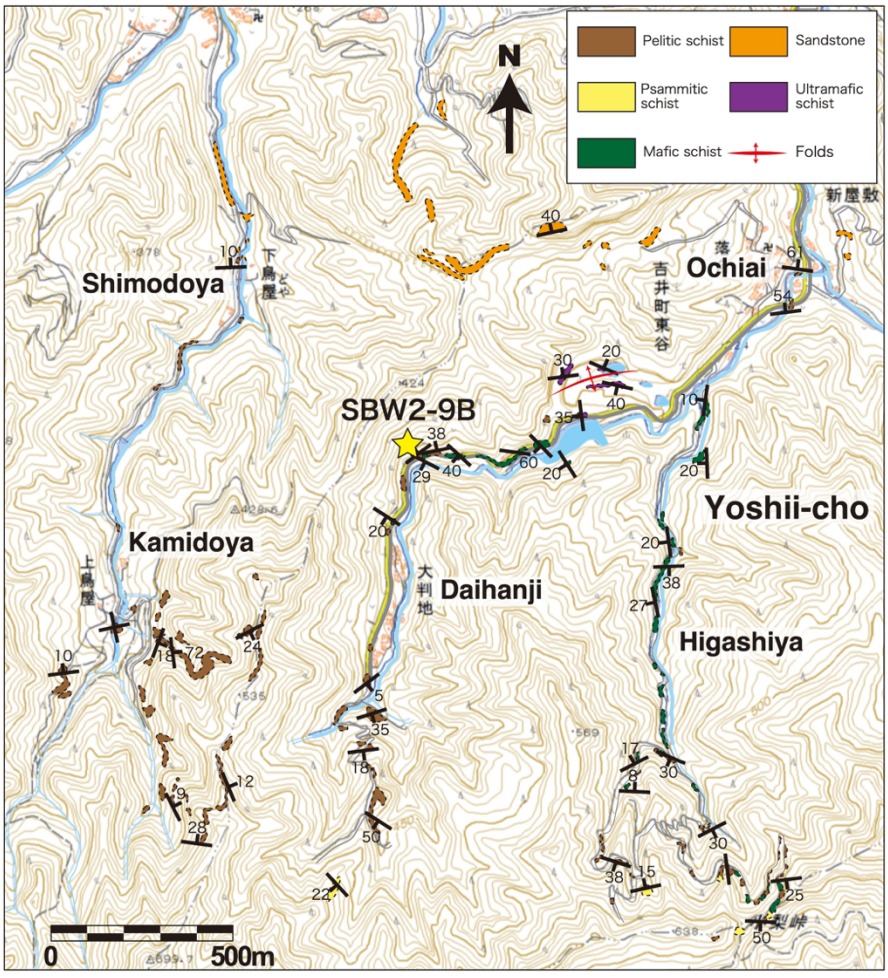

Fig. 2. A route map of the Sanbagawa metamorphic rocks in Yoshii area, Takasaki city, Kanto Mountains. Sample location of pelitic schist (sample SBW2-9B) discussed in this study is also shown. GPS coordinates of the samples and their mineral assemblages are listed in Appendix A and B, respectively.

Fig. 3. Field occurrence of pelitic schist and greenschist at locality SBW2-9.

Prefecture and compare the results with those from other regions. This is the first report of quantitative *P–T* condition estimated for the Sanbagawa schists from Kanto Mountains based on phase equilibrium modeling approach.

Petrography and mineral chemistry

The samples discussed in this study were collected from Yoshii area, west of Jushi-Kuroya Fault in Kanto Mountains (Fig. 1b). Totally forty-seven schist samples collected from the chlorite, garnet, and biotite zones were examined in detail. A route map of the studies area is shown in Figure 2. GPS coordinates of the samples discussed in this study and their mineral assemblages are listed in Appendix A and B, respectively. Representative electron microprobe data of minerals are shown in Appendix C.

We confirmed that chlorite ± garnet pelitic schists, which correspond to the chlorite- and garnet-zone samples, are abundant in the southern part of the study area, whereas chlorite + garnet + biotite pelitic schists (corresponding to a common assemblage of the biotite zone) occur in the northern part. Only one sample from the biotite zone (sample SBW2-9B, Fig. 3) contains both garnet and phengite. It is dark grayish in color, fine grained, well foliated, and composed of quartz (40–50%), phengite (20–30%), plagioclase (10–20%), and chlorite (5–10%) with minor biotite, epidote, garnet, apatite, ilmenite, and graphite (Figs. 4a,b). Fine-grained idioblastic garnet (0.01–0.03 mm) coexists with phengite, plagioclase, quartz, and epidote (Figs. 4c,d), although some garnet grains are completely included in plagioclase. It is Mn-rich (Mn/(Mg+Fe+Ca+Mn) = 0.63–0.78, X_{Mg} = Mg/(Fe+Mg) = 0.18–0.29), and spessartine component decreases, and almandine and grossular components increase from core ($Alm_{5\text{-}10}$ $Prp_{1\text{-}3}$ $Grs_{15\text{-}17}$ $Sps_{71\text{-}78}$) to rim ($Alm_{7\text{-}13}$ $Prp_{2\text{-}5}$ $Grs_{17\text{-}20}$ $Sps_{63\text{-}71}$). Plagioclase (nearly pure albite as $Ab_{99.2\text{-}100}$, Fig. 5) occurs as fine-grained subidioblastic to xenoblastic minerals associated with garnet and epidote in the matrix (0.1–0.5 mm) or as medium-grained spotted grains (0.5–1.0 mm)

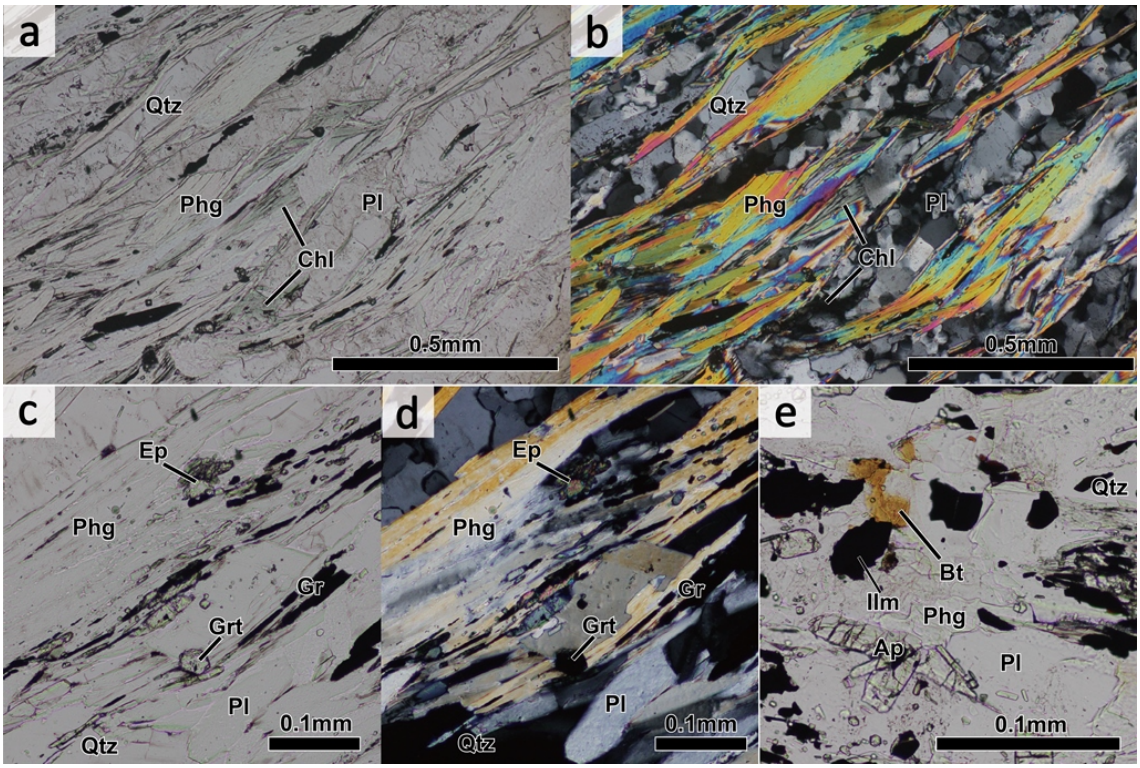

Fig. 4. (a–e) Thin section photographs of pelitic schist (sample SBW2-9B) discussed in this study. Qtz: quartz, Pl: plagioclase, Phg: phengite, Chl: chlorite, Gr: graphite, Ep: epidote, Grt: garnet, Bt: biotite, Ilm: ilmenite, Ap: apatite.

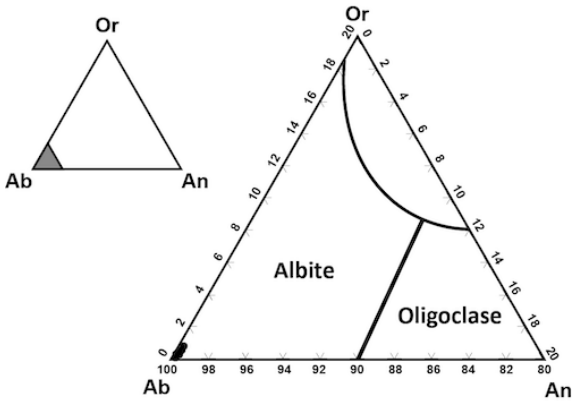

Fig. 5. A compositional diagram showing plagioclase chemistry.

(Figs. 4a-d). Coarse-grained lepidoblastic white mica (0.1–1.0 mm) coexists with garnet, plagioclase, quartz, epidote, chlorite, and biotite (Fig. 4a-d). It is phengitic with Si = 3.33–3.41 pfu, X_{Mg} = 0.52–0.59, and Na/(Na+K) = 0.02–0.12. Fine-grained subidioblastic epidote (0.01–0.02 mm) is often present as inclusions in plagioclase or in the matrix (Figs. 3c,d). Coarse-grained lepidoblastic chlorite (0.2–1.0 mm) is clinochlore in composition (Si = 5.82–5.85 pfu, X_{Mg} = 0.72–0.75, Fig. 6), possibly a product of retrograde metamorphism from fine-grained (0.01–0.03 mm) biotite.

P–T condition

The garnet-phengite geothermometer was applied to coexisting garnet and phengite in sample SBW2-9B (Figs. 4c,d). The estimated temperature range of the mineral pair is 480–580°C (at 8 kbar) based on the method of Krogh and Råheim (1978) which relies on experimental calibration of Fe-Mg fractionation between garnet and phengite. A calculated temperature range using the method of Wu et al. (2002) is 460–550°C (at 8 kbar). We could not estimate temperatures from other pelitic samples because of the lack of coexistence of garnet and phengite.

Metamorphic *P–T* conditions of the stability of mineral assemblages in sample SBW2-9B were further constrained using THERMOCALC 3.33 (Powell and Holland, 1988; updated October 2009) with an updated version of the internally consistent data set of Holland and Powell (1998; data set tcds55s, file created November 2003). The calculations were undertaken in the system MnO-Na_2O-CaO-K_2O-FeO-MgO-Al_2O_3-SiO_2-H_2O-TiO_2 (MnNCKFMASHT). Manganese was taken into account for the calculation because of high MnO content in garnet (~35 wt.% corresponding to up to 78 mol.% spessartine component) which probably affected the stability of the mineral assemblage. The phase considered in the modeling are garnet, biotite, and ilmenite (White et al., 2005), white mica (Coggon and Holland, 2002), plagioclase (Holland and Powell, 2003), and epidote (Holland and Powell, 1998). Rutile, quartz, H_2O, albite, and titanite are treated as pure end-member phases. The chemical composition (in wt.%) of the sample analyzed by XRF at Activation Laboratories, Canada, is SiO_2 = 60.38, Al_2O_3 = 17.73, FeO = 7.41, MnO = 0.45, MgO = 2.24, CaO = 0.97, Na_2O = 1.27, K_2O = 5.55, TiO_2 = 0.66, and P_2O_5 = 0.15. Water content was inferred as 11.14 mol.% based on LOI (loss on ignition) value (3.27 wt.%). All Fe was regarded as FeO because of the occurrence of graphite. As we excluded P_2O_5 from the system and the sample contains apatite (Fig. 4e), the CaO content equivalent to apatite was extracted from the calculation. Figure 7 is a *P–T* pseudosection for sample SBW2-9B showing the stability field of the peak assemblage (quartz + phengite + albite + biotite + epidote

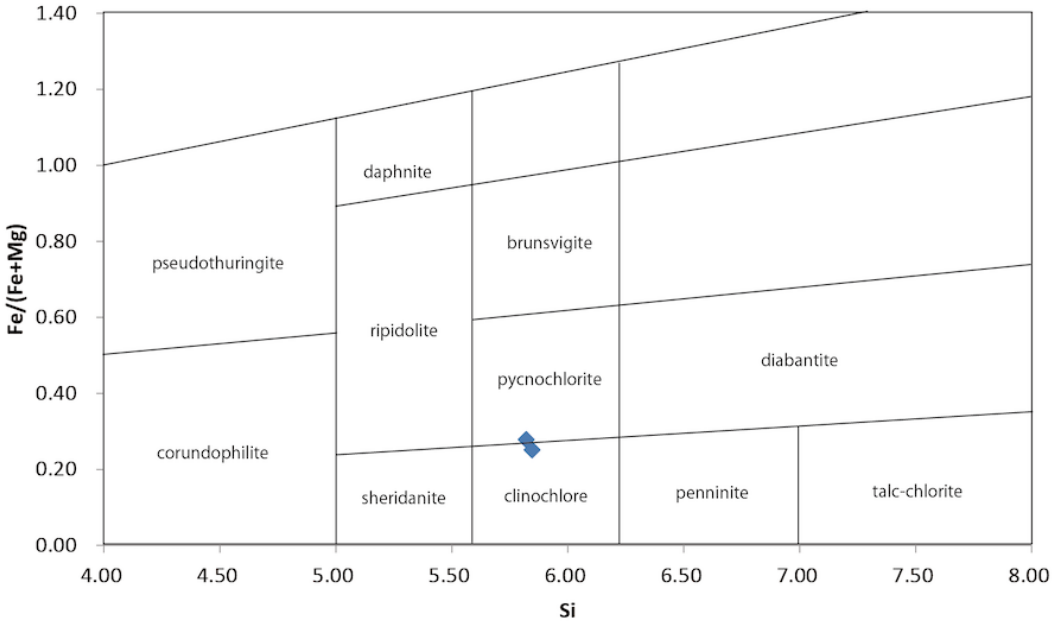

Fig. 6. A compositional diagram showing chlorite chemistry.

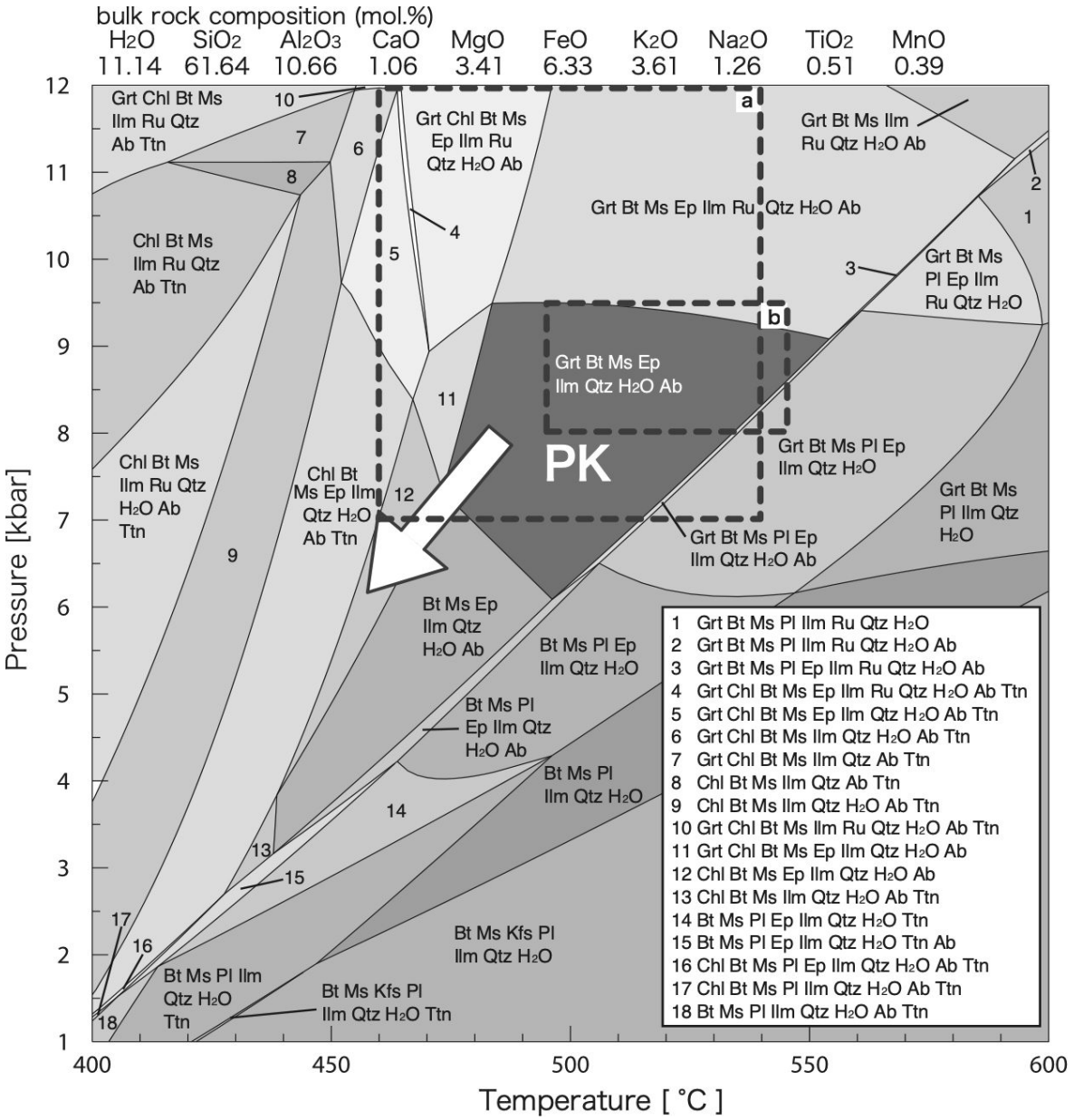

Fig. 7. *P-T* diagram showing a calculated pseudosection of mineral assemblages in sample SBW2-9B. 'PK' corresponds to the stability field of the peak mineral assemblage. Arrow indicates inferred retrograde *P–T* path. a: *P–T* condition after Hirajima (1989). b: *P–T* condition of albite-biotite zone in central Shikoku (Enami et al., 1994). See Figure 4 for mineral name abbreviation. Ab: albite, Ms: muscovite/phengite, Ttn: titanite, Rt: rutile.

+ garnet + ilmenite) at 470–550°C/6–9.5 kbar (area PK in Fig. 7). The upper-pressure stability limit is constrained by rutile-in line, whereas the lower limit by garnet-out line. The upper-temperature stability limit is constrained by plagioclase-in line, whereas the lower limit by chlorite-in line. As chlorite is stable at retrograde stage, a retrograde *P–T* path has been inferred as shown by an arrow in Figure 7.

Discussion

The Sanbagawa pelitic schists from Yoshii area examined in this study are comparable with those from the garnet zone, the chlorite zone, and the biotite zone in Kanto Mountains, which is consistent with the results of previous studies (e.g., Yano and Tagiri, 1998; Abe et al., 2001). The peak and retrograde mineral assemblages in sample SBW2-9B are quartz + phengite + albite + biotite + epidote + garnet + ilmenite and chlorite + biotite + muscovite + epidote + ilmenite + quartz + albite, respectively. The peak condition has been estimated as 470–550°C/6.0–9.5 kbar based on garnet-phengite geothermometry and phase equilibrium modeling in MnNCKFMASHT system (Fig. 4), which is nearly consistent with previous *P–T* estimates using carbon isotopic fractionation between calcite and graphite for Fe-Mn rich nodule and calcite-dolomite geothermometry

(460–540°C/7-12 kbar, Hirajima, 1989; box 'a' in Fig. 4) and Raman carbonaceous material thermometer for pelitic schist from the biotite zone (460–510°C, Kouketsu and Shimizu, 2014). The peak metamorphic event was followed by decompressional cooling toward the stability field of chlorite-bearing retrograde assemblage (<470ºC/<7 kbar) possibly along a clockwise *P–T* path.

The peak *P–T* conditions of the Sanbagawa schists in central Shikoku estimated in previous studies (e.g., Enami, 1983; Enami et al., 1994) are <360°C/5.5–6.5 kbar (chlorite zone), 425–455°C/7–8.5 kbar (garnet zone), 495–545°C/8–9.5 kbar (albite-biotite zone), and 585–635°C/9–11 kbar (oligoclase-biotite zone). The results of this study therefore confirmed the peak *P–T* condition of pelitic schists in Kanto Mountains is lower than that of the oligoclase-biotite zone in central Shikoku, but nearly consistent with the condition of the albite-biotite zone (box 'b' in Fig. 4), which is comparable with the previous model that the grade of metamorphism decreases from the western part (central Shikoku) to the eastern part (Kanto Mountains) of the belt (e.g., Hashimoto et al., 1990; Enami, 1994), suggesting a shallower level of the orogeny is exposed in Kanto Mountains possibly because of differential exhumation processes within the belt.

The Sanbagawa pelitic schists in Kii Peninsula and Sakuma-Tenryu area (Fig. 1a) contain mineral assemblages of chlorite + albite + muscovite ± garnet ± biotite (Wang and Maekawa, 1997; Tagiri et al., 2000) possibly equivalent to the chlorite zone, the garnet zone, and the biotite zone of Kanto Mountains. Those in Kyushu might correspond to the chlorite zone (Miyazaki and Yoshioka, 1992). However, it is difficult to quantitatively compare the results with those from Kanto Mountains and central Shikoku because of the lack of available *P–T* estimates from Kii, Sakuma-Tenryu, and Kyushu areas. Future application of phase equilibrium modeling technique on various pelitic schists from different regions would be useful for regional correlation of the Sanbagawa metamorphism.

Acknowledgements

Chemical analyses of minerals were carried out using an electron microprobe analyzer (JEOL JXA-8530F) at Chemical Analysis Division, University of Tsukuba. This study was partly supported by a Grant-in-Aid for Scientific Research from Japan Society for the Promotion of Science (JSPS) (No. 26302009, 18H01300, and 19F19020) to Tsunogae. We thank Dr. Sam Uthup for constructive review comments.

References

Abe, T., Takagi, H., Shimada, K., Kimura, S., Ikeyama, K., and Miyashita, A. (2001) Ductile shear deformation of the Sambagawa metamorphic rocks in the Kanto Mountains. *Journal of the Geological Society of Japan*, **107**, 337–353 (in Japanese with English abstract).

Banno, S. (1964) Petrologic studies on Sanbagawa crystalline schists in the Bessi-Ino district, central Sikoku, Japan. *Journal of the Faculty of Science, University of Tokyo, Section 2*, **15**, 203–319.

Coggon, R. and Holland, T.J.B. (2002) Mixing properties of phengitic micas and revised garnet-phengite thermobarometers. *Journal of Metamorphic Geology*, **20**, 683–696.

Enami, M. (1983) Petrology of pelitic schist in the oligoclase-biotite zone of the Sanbagawa metamorphic terrain, Japan: phase equilibria in the highest grade zone of a high-pressure intermediate type of metamorphic belt. *Journal of Metamorphic Geology*, **1**, 141–161.

Enami, M. (1994) Sanbagawa metamorphism: implication for evolution of a subduction zone. *Journal of Mineralogy, Petrology and Economic Geology*, **89**, 409–422 (in Japanese with English abstract).

Enami, M., Wallis, S.R., and Banno, Y. (1994) Paragenesis of sodic pyroxene-bearing quartz schists: intermediate type of metamorphic belt. *Journal of Metamorphic Geology*, **1**, 141–161.

Hashimoto, M., Tagiri, M., Masuda, K., and Kusakabe, K. (1990) Biotite zone of Sambagawa metamorphic terrane in Kanto Mountains (abs.), Abstracts, *The 96th Annual Meeting of the Geological Society of Japan*, 596–596 (in Japanese).

Higashino, T. (1975) Biotite zone of Sanbagawa metamorphic terrain in the Shiragayama area, central Shikoku, Japan. *Journal of Geological Society of Japan*, **81**, 653–670 (in Japanese with English abstract).

Higashino, T. (1990) The higher grade metamorphic zonation of the Sambagawa metamorphic belt in central Shikoku, Japan. *Journal of Metamorphic Geology*, **8**, 413–423.

Hirajima, T. (1989) Mineralogy of a Fe-Mn rich nodule from the Sanbagawa schist in the Kanto Mountains, Japan. *Journal of the Geological Society of Japan*, **95**, 817–833.

Holland, T.J.B. and Powell, R. (1998) An internally consistent thermodynamic dataset for phases of petrological interest. *Journal of Metamorphic Geology*, **16**, 309–343.

Holland, T.J.B. and Powell, R. (2003) Activity-composition relations for phases in petrological calculations: an asymmetric multicomponent formulation. *Contributions to Mineralogy and Petrology*, **145**, 492–501.

Inui, M., Izumi, R., Watanabe, T., 2017. Estimated peak metamorphic temperature of the Sanbagawa schists from Nagatoro area, Kanto Mountains, using Raman microspectrometry on carbonaceous materials. Transaction of the Kokushikan University School of Science and Engineering, **11**, 55–60.

Inui, M. and Tanifuji, Al. (2018) Spatial distribution of garnet indicating control of bulk rock chemistry in the Sanbagawa metamorphic rocks, Kanto Mountains,

Japan. *Journal of Mineralogical and Petrological Sciences*, **113**, 181–189.

Isozaki, Y. and Itaya, T. (1990) Chronology of Sanbagawa metamorphism. *Journal of Metamorphic Geology*, **8**, 401–411.

Kouketsu, Y. and Shimizu, I. (2014) Application of the Raman carbonaceous material thermometer to the Chichibu-Sanbagawa belt in the Kanto Mountains, Japan. *Abstract volume, 2014 Japan Geoscience Union Meeting, Japan Geoscience Union, Yokohama*, SMP46-05.

Krogh, E. J. and Råheim, A. (1978) Temperature and pressure dependence of Fe-Mg partitioning between garnet and phengite, with particular reference to eclogites. *Contributions to Mineralogy and Petrology*, **66**, 75–80.

Kurata, H. and Banno, S. (1974) Low-grade progressive metamorphism of pelitic schists of the Sazare area, Sanbagawa metamorphic terrain in central Sikoku, Japan. *Journal of Petrology*, **15**, 361–382.

Makimoto, H. and Takeuchi, K. (1992) Geology of the Yorii district. *Geological Sheet Map at 1: 50,000. Geological Survey of Japan*, 136p.

Miyashiro, A. (1961) Evolution of metamorphic belts. *Journal of Petrology*, **2**, 277–311.

Miyashita, A. (1998) Re-examination of "Geologic structure formed by tectonic stacking of sliced layer" in the Sanbagawa metamorphic rocks, Kanto Mountains. *Journal of the Geological Society of Japan*, **10**, 731–746 (in Japanese with English abstract).

Miyazaki, K. and Yoshioka, T. (1992) Geology of the Saganoseki district. *Geological Sheet Map at 1: 50,000. Geological Survey of Japan*, 40p (in Japanese with English abstract).

Nakano, T., Takeuchi, K., Kato, H., Sakai, A., Hamasaki, S., Hiroshima, T., and Komazawa, M. (1998) Geological Map, 1:200,000, Nagano. Geological Survey of Japan.

Ozaki, M., Makimoto, H., Sugiyama, Y., Mimura, K., Sakai, A., Kubo, K., Kato, H., Komazawa, M., Hiroshima, T., and Sudo, S. (2002) Geological Map, 1:200,000, Kofu. Geological Survey of Japan, AIST.

Powell, R. and Holland, T.J.B. (1988) An internally consistent dataset with uncertainties and correlations: 3. Applications to geobarometry, worked examples and a computer program. *Journal of Metamorphic Geology*, **6**, 173–204.

Sakamoto, T., Sakai, A., Hata, M., Unozawa, A., Hiroshima, T., Komazawa, M., and Murata, Y. (1987) Geological Map, 1:200,000, Tokyo. Geological Survey of Japan.

Sudo, S., Makimoto, H., Hata, M., Unozawa, A., Takizawa, F., Sakamoto, T., Komazawa, M., and Hiroshima, T. (1991) Geological Map, 1:200:000, Utsunomiya, Geological Survey of Japan.

Tagiri, M., Yago, Y. and Tanaka, A. (2000) Shuffled-cards structure and different P/T conditions in the Sanbagawa metamorphic belt, Sakuma-Tenryu area, central Japan. *Island Arc*, **9**, 188–203.

Toriumi, M. (1977) Metamorphism of the Southern Kanto Mountains – Its pressure condition. Sambagawa Belt (Hide, K. Ed.). Hiroshima University Press, Hiroshima, 217–221 (in Japanese with English abstract).

Wang, C. L. and Maekawa, H. (1997) Albite-biotite zone of the Sanbagawa metamorphic belt in the northwestern part of the Kii Peninsula, Japan. *Journal of Mineralogy, Petrology and Economic Geology*, **92**, 43–54 (in Japanese with English abstract).

White, R.W., Pomoroy, N.E., and Powell, R. (2005) An in-situ metatexite-diatexite transition in upper amphibolite facies rocks from Broken Hill, Australia. *Journal of Metamorphic Geology*, **23**, 579–602.

Wu, C.M., Wang, X.S., Yang C.h., Gend, Y.S. and Liu, F.L. (2002) Empirical garnet-muscovite geothermometry in metapelites. *Lithos*, **62**, 1–13.

Yano, T. and Tagiri, M. (1998) Geological and thermal structure of Sanbagawa metamorphic belt in the Sanbagawa river and Ayukawa river area, Kanto Mountains. *Journal of the Geological Society of Japan*, **104**, 442–453 (in Japanese with English abstract).

Appendix A. GPS coordinates of sample localities discussed in this study.

Sample No.	Co-ordinates		Lithology
	Longitude	Latitude	
SBW1-1	N 36°11'49"	E 138°59'38"	pelitic schist
SBW1-2	N 36°11'30"	E 138°57'60"	pelitic schist
SBW1-3	N 36°11'04"	E 138°56'26"	pelitic schist
SBW1-4A	N 36°10'40"	E 138°54'52"	pelitic schist
SBW1-4B	N 36°10'40"	E 138°54'52"	siliceous schist
SBW1-5	N 36°10'24"	E 138°54'46"	pelitic schist
SBW1-6A	N 36°10'06"	E 138°54'10"	mafic schist
SBW1-6B	N 36°10'06"	E 138°54'10"	mafic schist
SBW1-6C	N 36°10'06"	E 138°54'10"	mafic schist
SBW1-6D	N 36°10'06"	E 138°54'10"	mafic schist
SBW2-5	N 36°10'50"	E 138°52'22"	pelitic schist
SBW2-6	N 36°11'24"	E 138°52'56"	pelitic schist
SBW2-7	N 36°11'58"	E 138°53'37"	pelitic schist
SBW2-8	N 36°12'26"	E 138°56'60"	pelitic schist
SBW2-9B	N 36°12'48"	E 138°57'05"	pelitic schist
SBW3-1	N 36°12'56"	E 138°57'25"	ultramafic schist
SBW3-2A	N 36°11'08"	E 139°00'36"	psammitic schist
SBW3-2B	N 36°11'08"	E 139°00'36"	mafic schist
SBW3-3	N 36°11'04"	E 139°00'54"	pelitic schist
SBW3-4	N 36°11'39"	E 139°01'11"	pelitic schist
SBW3-5	N 36°11'47"	E 139°01'22"	mafic schist
SBW3-6	N 36°12'17"	E 139°02'02"	pelitic schist
SBW3-7A	N 36°09'17"	E 139°01'45"	pelitic schist
SBW3-7B	N 36°09'17"	E 139°01'45"	pelitic schist
SBW3-8A	N 36°09'16"	E 139°01'07"	mafic schist
SBW3-8B	N 36°09'16"	E 139°01'07"	pelitic schist
SBW3-10	N 36°09'51"	E 138°59'09"	pelitic schist
SBW3-11	N 36°09'34"	E 138°57'13"	pelitic schist
SBW3-12	N 36°09'25"	E 138°57'34"	pelitic schist
SBW4-1	N 36°12'12"	E 138°56'59"	psammitic schist
SBW4-2A	N 36°12'56"	E 138°57'22"	ultramafic schist
SBW4-2B	N 36°12'56"	E 138°57'22"	ultramafic schist
SBW4-3	N 36°12'17"	E 138°55'37"	pelitic schist
SBW4-4	N 36°12'10"	E 138°55'32"	pelitic schist
SBW5-1	N 36°11'55"	E 138°54'35"	mafic schist
SBW5-2	N 36°12'07"	E 138°55'24"	pelitic schist
SBW5-3	N 36°12'07"	E 138°53'48"	mafic schist
SBW6-1	N 36°11'08"	E 138°53'20"	mafic schist
SBW6-2	N 36°11'12"	E 138°53'35"	psammitic schist
SBW6-3	N 36°11'07"	E 138°54'12"	psammitic schist
SBW6-4	N 36°10'33"	E 138°54'28"	pelitic schist
SBW6-5	N 36°10'25"	E 138°54'25"	pelitic schist
SBW6-6	N 36°10'18"	E 138°54'24"	pelitic schist
SBW6-7	N 36°11'25"	E 138°59'30"	pelitic schist
SBW6-8	N 36°10'17"	E 139°00'19"	pelitic schist
SBW6-9	N 36°10'30"	E 138°59'11"	pelitic schist
SBW6-10	N 36°10'04"	E 138°57'27"	pelitic schist (Qtz vein)
SBW6-12	N 36°12'39"	E 139°00'24"	mafic schist

Appendix B. Mineral assemblages and modal abundance of minerals in the schistose rocks from the study area.

Sample No.	Rock type	Qtz	Pl	Ms	Chl	Grt	Bt	Hbl	Ep	Act	Cal	Spn	Rt	Tur	others
SBW1-1	pelitic schist	+++	++	++	++										
SBW1-2	pelitic schist	+++	++	++	+	+			+					+	FeTiOx+
SBW1-3	pelitic schist	+++	+++	++	+	+	+		+		+	+	+	+	FeTiOx+
SBW1-4A	pelitic schist	+++	++	+++	+	+	+						+		FeTiOx+
SBW1-4B	siliceous schist	+++	++	+	+	+									
SBW1-5	pelitic schist	+++	++	+	+										
SBW1-6A	mafic schist	++	+++	+	+			++	+	+					
SBW1-6B	mafic schist	+	+++	+	+			+++	+	+					
SBW1-6C	mafic schist	++	+++	++	+			+++	+	+					
SBW1-6D	mafic schist	++	+++	+	+			+++	+	+			+		
SBW2-5	pelitic schist	+++	++	+++					+				+		
SBW2-6	pelitic schist	+++	+++	+++	+				+						
SBW2-7	pelitic schist	+++	++	+++		+							+		
SBW2-8	pelitic schist	+++	++	+++											
SBW2-9B	pelitic schist	+++	++	++	+	+	+		+			+			FeTiOx, Ap
SBW3-1	ultramafic schist		+++		+			+++	+	+					
SBW3-2A	psammitic schist	+++	++	+											
SBW3-2B	mafic schist	+	+++	+				++	+	+					
SBW3-3	pelitic schist	+++	++	++	++	+			+						
SBW3-4	pelitic schist	+++	++	+++							+				
SBW3-5	mafic schist	+	+++	+	+			+++	+		+				
SBW3-6	pelitic schist	++	++	+++	+				+		+			+	
SBW3-7A	pelitic schist	++	++	++	++	+	+		+						
SBW3-7B	pelitic schist	+++	++	++	+	+			+						
SBW3-8A	mafic schist	+	+++		+			+++	+						
SBW3-8B	pelitic schist	+++	++	++	+	+			+						
SBW3-10	pelitic schist	++	+++	++	+	+			+						
SBW3-11	pelitic schist	+++	++	++	+										
SBW3-12	pelitic schist	+++	++	++	+				+						
SBW4-1	psammitic schist	+++	++	++		+			+				+		Zrn+
SBW4-2A	ultramafic schist		+++		+			+++	+	+	+				
SBW4-2B	ultramafic schist		++					+++	+	+					
SBW4-3	pelitic schist	+++	++	++	+	+			+		+				
SBW4-4	pelitic schist	+++	++	+	+		+		+						
SBW5-1	mafic schist		+++	+	+			++							
SBW5-2	pelitic schist	+++	++	+	+	+			+						
SBW5-3	mafic schist		++		+			+++	+						
SBW6-1	mafic schist	+	+++		+			++	+						
SBW6-2	psammitic schist	+++	++	++		+			+						
SBW6-3	psammitic schist	+++	++	+	++	+									Zrn+
SBW6-4	pelitic schist	+++	++	+	++									+	
SBW6-5	pelitic schist	++	++												graphite+++
SBW6-6	pelitic schist	+++	+	++											graphite++
SBW6-7	pelitic schist	+++	++	+											graphite++
SBW6-8	pelitic schist	+++	++	++											
SBW6-9	pelitic schist	++	++	+++	+				+						
SBW6-10	pelitic schist (Qtz vein)	++	++	+++	+				+						
SBW6-12	mafic schist		+++					++	+	+	+				

+	0–10%
++	10–30%
+++	>30%

Appendix C-1. Representative electron microprobe data of garnet and plagioclase discussed in this study.

Sample No.	SBW2-9B	SBW2-9B	SBW1-3	SBW1-3	SBW1-3	SBW1-3	SBW2-9B	SBW2-9B	SBW2-9B	SBW2-9B
Mineral name	Garnet						Plagioclase			
No. oxygen	12	12	12	12	12	12	8	8	8	8
Remarks	Core	Rim	Core	Rim	Core	Rim	Core	Core	Rim	Rim
SiO_2	36.28	37.29	37.24	37.22	36.95	37.93	68.86	69.21	69.44	69.49
Al_2O_3	19.15	19.11	20.66	20.73	20.85	21.06	19.28	19.25	19.57	19.25
TiO_2	0.39	0.31	0.21	0.19	0.18	0.06	0.07	0.00	0.00	0.00
Cr_2O_3	0.00	0.00	0.00	0.08	0.00	0.01	0.00	0.00	0.00	0.03
FeO	2.32	5.29	13.16	16.75	13.33	22.06	0.00	0.02	0.00	0.01
MnO	35.88	30.87	24.29	19.83	23.48	12.73	0.03	0.00	0.00	0.01
MgO	0.28	1.43	0.18	0.22	0.14	0.38	0.00	0.05	0.04	0.02
CaO	5.58	5.27	5.93	6.51	6.43	7.20	0.12	0.09	0.03	0.02
Na_2O	0.04	0.07	0.00	0.05	0.00	0.22	11.69	11.90	11.90	12.15
K_2O	0.05	0.41	0.02	0.00	0.00	0.00	0.04	0.04	0.05	0.04
Total	99.96	100.03	101.69	101.58	101.35	101.63	100.09	100.57	101.04	101.01
Si	2.987	3.034	2.989	2.985	2.973	3.017	3.004	3.006	3.001	3.007
Al	1.858	1.832	1.954	1.959	1.977	1.974	0.991	0.985	0.997	0.981
Ti	0.024	0.019	0.012	0.011	0.011	0.004	0.002	0.000	0.000	0.000
Cr	0.000	0.000	0.000	0.005	0.000	0.001	0.000	0.000	0.000	0.001
Fe2+	0.160	0.360	0.883	1.123	0.897	1.467	0.000	0.001	0.000	0.000
Mn	2.501	2.127	1.651	1.347	1.600	0.858	0.001	0.000	0.000	0.000
Mg	0.034	0.173	0.021	0.026	0.017	0.045	0.000	0.003	0.002	0.002
Ca	0.492	0.459	0.510	0.559	0.554	0.613	0.006	0.004	0.002	0.001
Na	0.006	0.011	0.000	0.007	0.000	0.033	0.988	1.002	0.996	1.019
K	0.005	0.042	0.002	0.000	0.000	0.000	0.002	0.002	0.003	0.002
Total	8.066	8.057	8.023	8.025	8.028	8.010	4.994	5.004	5.000	5.013
Mg/(Fe+Mg)	0.176	0.324	0.024	0.023	0.018	0.030				
Alm (mole%)	5.0	11.5	28.8	36.8	29.2	49.2				
Prp (mole%)	1.1	5.5	0.7	0.9	0.5	1.5				
Grs (mole%)	15.4	14.7	16.6	18.3	18.1	20.6				
Sps (mole%)	78.5	68.2	53.9	44.1	52.2	28.8				
An (mole%)							0.6	0.4	0.2	0.1
Ab (mole%)							99.2	99.4	99.6	99.7
Or (mole%)							0.2	0.2	0.3	0.2

Appendix C-2. Representative electron microprobe data of phengite discussed in this study.

Sample No.	SBW2-9B	SBW2-9B	SBW2-9B	SBW1-3	SBW1-3	SBW1-2	SBW1-2	SBW1-4A
Mineral name	Phengite							
No. oxygen	11	11	11	11	11	11	11	11
Remarks	Core	Core	Around Ab					
SiO_2	49.41	48.65	49.53	48.43	48.26	48.48	49.09	49.63
Al_2O_3	24.91	26.78	26.71	31.58	31.87	30.20	28.81	26.52
TiO_2	0.31	0.43	0.29	0.36	0.31	0.22	0.07	0.10
Cr_2O_3	0.02	0.00	0.00	0.02	0.00	0.04	0.03	0.02
FeO	5.34	4.64	3.78	2.03	1.80	2.82	2.44	4.50
MnO	0.14	0.09	0.03	0.05	0.06	0.10	0.03	0.16
MgO	3.31	2.81	3.01	1.61	1.56	2.17	2.23	3.12
CaO	0.00	0.01	0.06	0.00	0.00	0.00	0.00	0.01
Na_2O	0.12	0.25	0.84	0.15	0.23	0.26	0.20	0.10
K_2O	10.82	11.05	9.79	10.51	10.51	10.27	10.13	9.85
Total	94.38	94.70	94.04	94.74	94.60	94.56	93.02	94.00
Si	3.400	3.330	3.374	3.244	3.235	3.268	3.348	3.386
Al	2.020	2.159	2.144	2.493	2.517	2.399	2.315	2.132
Ti	0.016	0.022	0.015	0.018	0.016	0.011	0.004	0.005
Cr	0.001	0.000	0.000	0.001	0.000	0.002	0.001	0.001
Fe2+	0.307	0.265	0.215	0.114	0.101	0.159	0.139	0.257
Mn	0.008	0.005	0.002	0.003	0.003	0.006	0.002	0.009
Mg	0.339	0.287	0.306	0.160	0.156	0.218	0.227	0.317
Ca	0.000	0.000	0.004	0.000	0.000	0.000	0.000	0.001
Na	0.015	0.034	0.111	0.020	0.029	0.034	0.026	0.013
K	0.950	0.964	0.850	0.898	0.898	0.883	0.881	0.857
Total	7.056	7.067	7.021	6.950	6.955	6.979	6.943	6.977
Mg/(Fe+Mg)	0.524	0.520	0.587	0.585	0.607	0.578	0.620	0.553

Appendix C-3. Representative electron microprobe data of chlorite and epidote discussed in this study.

Sample No.	SBW2-9B	SBW2-9B	SBW1-3	SBW1-3	SBW1-2	SBW1-4A	SBW2-9B	SBW2-9B
Mineral name	Chlorite						Epidote	
No. oxygen	28	28	28	28	28	28	12	12
Remarks	Core	Rim	Core	Rim	Core	Core	Core	Core
SiO_2	28.89	28.27	25.47	23.97	25.20	25.09	37.36	38.41
Al_2O_3	19.00	18.39	20.27	19.92	20.46	19.94	20.08	22.70
TiO_2	0.01	0.01	0.00	0.03	0.06	0.00	3.55	0.01
Cr_2O_3	0.03	0.00	0.07	0.05	0.03	0.00	0.00	0.00
Fe_2O_3							12.79	13.88
FeO	13.52	14.86	28.52	27.55	27.65	28.52		
MnO	2.00	2.47	1.40	1.29	0.88	1.16	1.96	1.47
NiO	0.14	0.15	0.00	0.02	0.00	0.00		
MgO	22.65	21.62	11.50	10.41	12.47	11.35	0.06	0.02
CaO	0.07	0.04	0.00	0.00	0.00	0.00	21.81	21.98
Na_2O	0.03	0.02	0.04	0.00	0.00	0.00	0.04	0.03
K_2O	0.00	0.00	0.00	0.01	0.00	0.03	0.05	0.00
Total	86.33	85.84	87.28	83.24	86.75	86.08	97.69	98.49
Si	5.846	5.822	5.527	5.460	5.464	5.525	2.890	2.927
Al	4.531	4.463	5.181	5.348	5.228	5.173	1.830	2.039
Ti	0.001	0.002	0.000	0.006	0.010	0.000	0.206	0.000
Cr	0.005	0.000	0.013	0.008	0.005	0.000	0.000	0.000
Fe3+	0.000	0.000	0.000	0.000	0.000	0.000	0.744	0.796
Fe2+	2.288	2.558	5.173	5.247	5.014	5.250	0.000	0.000
Mn	0.343	0.430	0.257	0.249	0.161	0.216	0.128	0.095
Ni	0.022	0.025	0.000	0.003	0.000	0.000		
Mg	6.829	6.632	3.717	3.533	4.027	3.721	0.007	0.003
Ca	0.015	0.009	0.000	0.000	0.000	0.000	1.807	1.794
Na	0.012	0.008	0.016	0.000	0.000	0.000	0.006	0.004
K	0.000	0.000	0.001	0.003	0.001	0.007	0.004	0.000
Total	19.891	19.949	19.885	19.857	19.910	19.892	7.622	7.657
Mg/(Fe+Mg)	0.749	0.722	0.418	0.402	0.445	0.415		